Progress In Electromagnetics Research B, Vol. 47, 107–126, 2013

ENERGY ESTIMATION BASED TR-MUSIC MICROWAVE IMAGING FOR EXTENDED TARGETS

Guangfu Zhang[1, *], Williams Weiji Wang[2], and Wei Wang[2]

[1]School of Electronic Science and Engineering, National University of Defense Technology, Changsha 410073, China

[2]Biomedical Engineering Group, University of Sussex, Brighton, BN1 9QT, United Kingdom

Abstract—A simple and effective double-thresholding strategy based on energy estimation is proposed to choose the optimal boundary between the signal subspace and noise subspace in TR-MUSIC algorithm for microwave imaging of extended targets. Simulations and imaging results are given to demonstrate its strong noise rejection and super-resolution capability. In the new method, the shape details of extended targets can be obtained from single frequency or multi-frequency scattering data.

1. INTRODUCTION

According to the American Cancer Society, breast cancer has become the first cancer killer for women, compared with other kinds of cancers in females [1]. Traditional techniques, such as X-ray mammography, magnetic resonance imaging (MRI) and Ultrasound (US), limit themselves in sensitivity, specificity and accuracy in the detection and diagnostic of malignant tumor. Thus many new methods and modalities, including electromagnetic techniques such as electrical impedance tomography (EIT) and microwave imaging techniques [2], have been proposed to overcome these limitations.

Motivated by the high contrast between malignant tumor tissue and the normal surrounding breast tissue in electrical properties (such as permittivity and conductivity), microwave imaging technology has attracted much attention because it is non-ionizing, more comfortable, more accurate and less expensive [3]. Except for common hardware components, such as signal generator, antenna array and data

Received 5 October 2012, Accepted 21 December 2012, Scheduled 25 December 2012

* Corresponding author: Guangfu Zhang (guangfuz818@hotmail.com).

sampling equipments (for example, vector network analyser (VNA) or oscilloscope), imaging algorithm and software play a very important role on the performance and detection capability of microwave imaging system.

There are two main modalities for microwave imaging the interior of the breast: (i) microwave tomography (MWT) and (ii) radar-based imaging. In MWT, a reconstruction of the electrical properties of the breast at each pixel is calculated iteratively by optimizing a cost function after a regularization procedure to solve the inherently ill-posed and nonlinear inverse electromagnetic problem, so it is time and resource-consuming. On the other hand, in radar-based imaging, signal processing techniques are employed to identify only the regions with stronger backscattering, which indicate the presence of a contrast in electrical properties. Many signal processing methods have been adopted to complete this task, including wavefront reconstruction [4], delay and sum (DAS) beamformer or confocal microwave imaging (CMI) [5–7], microwave imaging via space-time (MIST) beamforming [8], multi-input multi-output (MIMO) radar processing techniques [9], and subspace-based Time-reversal MUtiple SIgnal Classification (TR-MUSIC) algorithm [10–17].

Because of its super-resolution capability [17], subspace-based TR-MUSIC algorithm has obtained more attentions in point and extended targets imaging. In Ref. [10], H. Lev-Ari and A. J. Devaney related the time-reversal field and subspace-based signal processing of multi-static data together at the first time and proposed a subspace-based method, later called TR-MUSIC algorithm, for point targets location within the framework of the Born approximation. F. K. Gruber et al. further showed that TR-MUSIC algorithm can be used to locate point targets even if considering the multiple scattering between them [11, 12]. S. Hou et al. applied this method to extended targets and concluded that the imaging function would peak not only on the illuminated boundary parts, but also peak inside the domain, and proposed a new explanation of imagine peak points [13]. E. A. Marengo et al. developed TR-MUSIC-based imaging theory of extended scatters and proposed the concepts of "effective signal subspace" and "effective noise subspace" for extended targets [14]. These achievements revealed that TR-MUSIC can be applied to extended targets as same as point targets and the shape details can be obtained. Furthermore, TR-MUSIC algorithm can be used to other applications, such as through-the-wall imaging (TWI) [15] and surveillance in wireless sensor network [16].

In general, the malignant tumor tissue and the normal surrounding breast tissue exhibit as extended targets to microwave frequency

band due to their electrical dimension and heterogeneity feature. Due to distributed scattering and measurement noise, the multi-static response matrix of extended targets is full rank, but not rank-deficient as point targets. Because there is no obvious boundary between signal subspace and noise subspace, TR-MUSIC can't be executed directly. To resolve this problem for extended target imaging, E. A. Marengo et al. took the "knee" of the singular value spectrum in logarithmic scale as the boundary point to pick the principal components out from the noised signal subspace [14]. And S. Hou et al. proposed a more complicated resolution and noise level based thresholding strategy for regularization, but multiple-frequency data is needed [13].

According to our numerical tests using the scattered data of simple extended targets from FDTD simulation, the above two methods can't obtain the best imaging results. We find that the acceptable imaging results happen at multiple boundary points but not at one specific point and that at most time these boundary points are not the "knee" of the singular value spectrum. The super-resolution property of TR-MUSIC can guarantee a good imaging even only from single frequency data. Therefore, we propose a new double-thresholding strategy based on energy estimation to decide the best boundary region between effective signal subspace and noise subspace and combine all the effective boundary points together to obtain a more distinct image of illuminated area. Although only the 2D scenarios are simulated, the algorithm itself is suitable for 3D imaging.

This paper is organized as follows. In Section 2, the energy estimation based TR-MSIC algorithm is deduced in detail under the condition of imaging geometry and configuration and the final imaging function formula is obtained. Then the simulations and imaging results for point targets, rectangle metal cylinder and irregular metal cylinder are presented in Section 3, respectively, with the analysis and discussion about noise rejecting performance, super-resolution capability and multi-frequency data fusion imaging. Section 4 is devoted to the conclusions.

2. ENERGY ESTIMATION BASED TR-MUSIC ALGORITHM

The imaging geometry and configuration is demonstrated in Figure 1. The object is located inside the imaging region $X \times Y$, which is surrounded by a uniform circular N-element array with radius R. Each element antenna transmits in turn electromagnetic wave towards the imaging region and all the element antennas receive the scattered

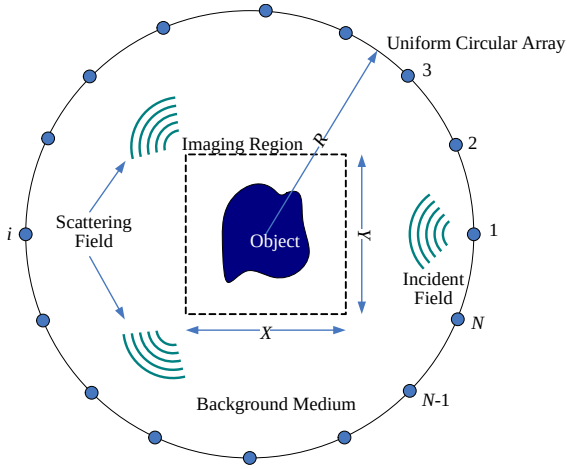

Figure 1. Imaging geometry and configuration.

wavefront. This means that each antenna is a transducer. The obtained scattering data matrix is then processed to reconstruct the position and shape of the object located in the imaging region.

2.1. Time-reversal (TR) Principle

As stated in Ref. [15], in lossless and stationary medium, the electromagnetic field component $E(\mathbf{x}, t)$ satisfies the following scalar wave equation

$$\nabla^2 E(\mathbf{x}, t) - \mu\varepsilon \frac{\partial^2}{\partial^2 t} E(\mathbf{x}, t) = 0 \tag{1}$$

where $\mathbf{x}$ denotes the space position vector, t the time, and μ and ε the permeability and permittivity of the medium, respectively. The quadratic differential relationship between field strength and time in Eq. (1) keeps the invariance to the sign of time, upon which the concept of time-reversal is based. That is, if $E(\mathbf{x}, t)$ is the solution to Eq. (1), its time-reversal field $E(\mathbf{x}, -t)$ is also a solution to the same equation.

The wave propagation process means that $E(\mathbf{x}, -t)$ would precisely retrace the path of the original wave $E(\mathbf{x}, t)$. If $E(\mathbf{x}, t)$ is the divergent scattered field, then $E(\mathbf{x}, -t)$ is the convergent wave which will focus on the source with TR process. In frequency domain, TR process can be implemented by using the phase conjugation $E^*(\mathbf{x}, \omega)$ to replace $E(\mathbf{x}, \omega)$, where the superscript star denotes the complex conjugation and $E(\mathbf{x}, \omega)$ is the Fourier transform of $E(\mathbf{x}, t)$.

2.2. Multi-static Frequency Response Matrix (MFRM) and TR-MUSIC Algorithm for Point Targets

For the array of N transducers in Figure 1, define the inter-element impulse response $h_{ij}(t)$ to be the signal received at the ith transducer with an impulse sent out from the jth transducer, $i, j = 1, 2, \ldots, N$, the matrix

$$\mathbf{H}(t) = [h_{ij}(t)]_{N\times N} \tag{2}$$

is called the multi-static response matrix in time domain. Due to the space reciprocity of stationary medium, $\mathbf{H}(t)$ is symmetric, i.e., $h_{ij}(t) = h_{ji}(t)$.

For an exciting source signal vector

$$S(t) = [s_1(t), s_2(t), \ldots, s_N(t)]^T \tag{3}$$

where superscript T denotes transpose, and the received signal vector of the array is

$$R(t) = [r_1(t), r_2(t), \ldots, r_N(t)]^T = \mathbf{H}(t) \otimes S(t) \tag{4}$$

where the sign $\otimes$ denotes convolution in time domain. In the frequency domain, it becomes

$$R(\omega) = \mathbf{H}(\omega) S(\omega) \tag{5}$$

where $\mathbf{H}(\omega)$ is the Fourier transform of $\mathbf{H}(t)$ and called multi-static frequency response matrix (MFRM).

If the exciting signal is a single frequency signal, i.e., ω_0, the MFRM $\mathbf{H}(\omega_0)$, denoted by $\mathbf{H}$ since now, has the following singular value decomposition (SVD)

$$\mathbf{H} = \mathbf{U}\mathbf{\Sigma}\mathbf{V}^{\dagger} \tag{6}$$

with Q non-zero singular values $\sigma_1 \geq \sigma_2 \geq \ldots \sigma_Q \geq 0$, where $Q = \text{rank}(\mathbf{H})$, $\mathbf{\Sigma} = \text{diag}\{\sigma_1, \sigma_2, \ldots \sigma_Q, 0, \ldots, 0\}$ is a $N \times N$ diagonal matrix, the superscript $\dagger$ denotes complex conjugation transpose. $\mathbf{U}$ and $\mathbf{V}$ are unitary matrices and their columns are called left singular vectors and right singular vectors, respectively. The first Q columns and the last $N - Q$ columns of $\mathbf{V}$ span the row space and nullspace of $\mathbf{H}$, respectively. The first Q columns and the last $N - Q$ columns of $\mathbf{U}$ span the row space and nullspace of $\mathbf{H}^T$, respectively [18]. That is

$$\begin{aligned} \text{null}(\mathbf{H}) &= \text{span}\{\nu_{Q+1}, \ldots, \nu_N\} \triangleq \mathbf{V}_{N-Q} \\ \text{range}\left(\mathbf{H}^T\right) &= \text{span}\{\nu_1, \ldots, \nu_Q\} \triangleq \mathbf{V}_Q \\ \text{range}(\mathbf{H}) &= \text{span}\{\mu_1, \ldots, \mu_Q\} \triangleq \mathbf{U}_Q \\ \text{null}\left(\mathbf{H}^T\right) &= \text{span}\{\mu_{Q+1}, \ldots, \mu_N\} \triangleq \mathbf{U}_{N-Q} \end{aligned} \tag{7}$$

where μ_k and ν_k is the kth column vector of $\mathbf{U}$ and $\mathbf{V}$, respectively. Because $\mathbf{H} = \mathbf{H}^T$ and $\text{null}(\mathbf{H})^{\perp} = \text{range}(\mathbf{H}^T)$, it can be shown that $\mathbf{U}_Q$ is the orthogonal complement of $\mathbf{V}_{N-Q}$ and $\mathbf{V}_Q$ is the orthogonal complement of $\mathbf{U}_{N-Q}$, respectively.

The electromagnetic wave propagation is dominated by the Green's function $g_0(\mathbf{x}_1, \mathbf{x}_2)$ of the background medium, where $\mathbf{x}_1$ denotes the field point and $\mathbf{x}_2$ the source point. Due to spatial reciprocity, $\mathbf{x}_1$ and $\mathbf{x}_2$ can be exchanged, that is, $g_0(\mathbf{x}_1, \mathbf{x}_2) = g_0(\mathbf{x}_2, \mathbf{x}_1)$.

Assume that there are M point scatterers located at $\mathbf{x}_1, \mathbf{x}_2, \ldots, \mathbf{x}_M$ in the imaging region with isotropic reflectivity τ_m, $m = 1, 2, \ldots, M$, and the array element antennas locate at $\boldsymbol{\xi}_1, \boldsymbol{\xi}_2, \ldots, \boldsymbol{\xi}_N$, respectively. If Born approximation is applied, i.e., neglecting the multiple scattering between the point scatterers, $\mathbf{H}$ can be written as

$$\begin{aligned}\mathbf{H} &= \begin{bmatrix} \sum_{m=1}^{M} g_0(\boldsymbol{\xi}_1,\mathbf{x}_m)\tau_m g_0(\mathbf{x}_m,\boldsymbol{\xi}_1) & \cdots & \sum_{m=1}^{M} g_0(\boldsymbol{\xi}_1,\mathbf{x}_m)\tau_m g_0(\mathbf{x}_m,\boldsymbol{\xi}_N) \\ \vdots & \ddots & \vdots \\ \sum_{m=1}^{M} g_0(\boldsymbol{\xi}_N,\mathbf{x}_m)\tau_m g_0(\mathbf{x}_m,\boldsymbol{\xi}_1) & \cdots & \sum_{m=1}^{M} g_0(\boldsymbol{\xi}_N,\mathbf{x}_m)\tau_m g_0(\mathbf{x}_m,\boldsymbol{\xi}_N) \end{bmatrix} \\ &= \sum_{m=1}^{M} \tau_m G_0(\mathbf{x}_m) G_0^T(\mathbf{x}_m) \end{aligned} \tag{8}$$

where $G_0(\mathbf{x}_m)$ is called illumination vector for $\mathbf{x}_m$, $m = 1, 2, \ldots, M$, defined by

$$G_0(\mathbf{x}_m) = [g_0(\boldsymbol{\xi}_1, \mathbf{x}_m), g_0(\boldsymbol{\xi}_2, \mathbf{x}_m), \ldots, g_0(\boldsymbol{\xi}_N, \mathbf{x}_m)]^T \tag{9}$$

According to Eq. (8), it is clear that $\mathbf{H}$ is a linear combination of M illumination vectors $G_0(\mathbf{x}_1)$, $G_0(\mathbf{x}_2)$, $\ldots$, $G_0(\mathbf{x}_M)$, and furthermore, $\text{rank}(\mathbf{H}) = M$ if $M < N$.

For the case of $M < N$, $\mathbf{U}_M$ is called the signal subspace $\mathbf{V}^S$ and $\mathbf{V}_{N-M}$ is called the noise subspace $\mathbf{V}^N$ in MUSIC algorithm. According to Eq. (7), $\mathbf{V}^N$ spans the nullspace of $\mathbf{H}$ and is the orthogonal complement of $\mathbf{V}^S$. For arbitrary search point $\mathbf{x}$ in the imaging region, its illumination vector is $G_0(\mathbf{x})$. if $\mathbf{x}$ collocates with any point among $\mathbf{x}_1, \mathbf{x}_2, \ldots, \mathbf{x}_M$, then $G_0(\mathbf{x})$ belongs to $\mathbf{V}^S$ and its projection length to $\mathbf{V}^N$, $\|P_{V^N} G_0(\mathbf{x})\|_2$, equals to zero, otherwise $\|P_{V^N} G_0(\mathbf{x})\|_2$ is finite, where $\|\ \|_2$ denotes Euclidean norm. A pseudo-

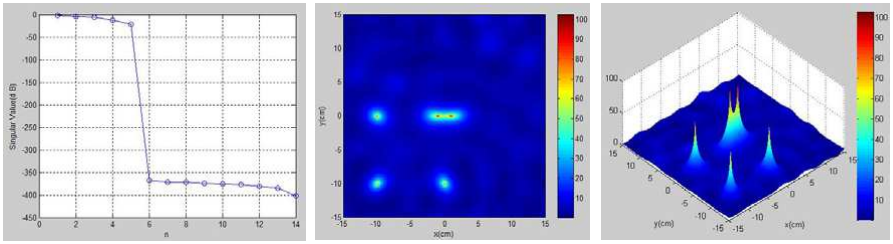

Figure 2. Multiple point targets imaging.

spectral imaging function can be constructed as

$$I(\mathbf{x}) = \frac{1}{\|P_{V^N} G_0(\mathbf{x})\|_2^2} = \left[\sum_{k=M+1}^{N} \left| \nu_k^{\dagger} G_0(\mathbf{x}) \right|^2 \right]^{-1}$$

$$= \frac{1}{\|G_0(\mathbf{x})\|_2^2 - \|P_{V^S} G_0(\mathbf{x})\|_2^2} = \left[\|G_0(\mathbf{x})\|_2^2 - \sum_{k=1}^{M} \left| \mu_k^{\dagger} G_0(\mathbf{x}) \right|^2 \right]^{-1} \quad (10)$$

This is called subspace-based MUSIC algorithm. When $\mathbf{x}$ collocates with the point target position, $I(\mathbf{x})$ will be great rather than theoretical infinity because of measurement noise or computation error. Therefore, $I(\mathbf{x})$ will peak greatly at the positions of point targets and super-resolution characteristic can be expected, which is demonstrated in Figure 2.

In the history of MUSIC algorithm, the Hermitian operator $\mathbf{K}_t = \mathbf{H}^{\dagger}\mathbf{H}$ is also called transmit-mode time-reversal operator, and $\mathbf{K}_r = \mathbf{H}\mathbf{H}^{\dagger}$ is called receive-mode time-reversal operator [20]. Because $\mathbf{K}_t S(\omega) = \mathbf{H}^{\dagger}\mathbf{H}S(\omega) = \mathbf{H}^{\dagger}R(\omega)$ means the received signals are back propagated after phase conjugated, toward the source positions where they come from, according to the TR principle mentioned above. And the eigenvectors of matrix $\mathbf{K}_t$ can be shown to correspond to the point targets in a one-to-one manner [10]. On the other hand, it can be shown that the orthonormal columns of $\mathbf{U}$ and $\mathbf{V}$ are the eigenvectors of $\mathbf{K}_r$ and $\mathbf{K}_t$, respectively. Therefore, the singular vectors of $\mathbf{H}$ play the same role as the eigenvectors of $\mathbf{K}_r$ or $\mathbf{K}_t$. Because subspace-based MUSIC blends ideas of standard MUSIC with the eigenvalue decomposition of the time-reversal operator, it is also called TR-MUSIC method [14, 15].

Mathematically and practically, SVD of $\mathbf{H}$ is preferred to eigenvalue decomposition (ED) of $\mathbf{K}_r$ or $\mathbf{K}_t$, because: (i) SVD uses orthonormal bases whereas ED uses a basis that generally is not

orthonormal; (ii) All matrices (even rectangular ones) have a SVD and not all matrices (even square ones) have an ED [19].

If the array consists of two different sets of transmitters and receivers, e.g., there are N_t transmitters located at $\boldsymbol{\xi}_1$, $\boldsymbol{\xi}_2$, ..., $\boldsymbol{\xi}_{N_t}$ and there are N_r receivers located at η_1, η_2, ..., η_{N_r}. The response matrix for M point targets located at $\mathbf{x}_1$, $\mathbf{x}_2$, ..., $\mathbf{x}_M$ with reflectivity τ_1, ..., τ_M becomes

$$\mathbf{H} = \sum\nolimits_{m=1}^{M} \tau_m G_{0T}\left(\mathbf{x}_m\right) G_{0R}^{T}\left(\mathbf{x}_m\right) \tag{11}$$

where

$$G_{0R}\left(\mathbf{x}_m\right) = \left[g_0\left(\boldsymbol{\xi}_1,\mathbf{x}_m\right), g_0\left(\boldsymbol{\xi}_2,\mathbf{x}_m\right), \ldots, g_0\left(\boldsymbol{\xi}_{N_r},\mathbf{x}_m\right)\right]^T$$

and

$$G_{0T}\left(\mathbf{x}_m\right) = \left[g_0\left(\mathbf{x}_m,\boldsymbol{\xi}_1\right), g_0\left(\mathbf{x}_m,\boldsymbol{\xi}_2\right), \ldots, g_0\left(\mathbf{x}_m,\boldsymbol{\xi}_{N_t}\right)\right]^T$$

where $m = 1, 2, \ldots, M$, are illumination vectors for the receiver and transmitter arrays respectively. It can be shown that $G_{0T}(\mathbf{x}_m)$, $m = 1, 2, \ldots, M$, are the left singular vectors for $\mathbf{H}$ and span the column signal subspace V_C^S. Similarly, $G_{0R}\left(\mathbf{x}_m\right)$, $m = 1, 2, \ldots, M$, are the right singular vectors for $\mathbf{H}$ and span the row signal subspace V_R^S. The MUSIC imaging function can be constructed using both of them [17, 20]

$$\begin{aligned} I\left(\mathbf{x}\right) &= \left[\left\|P_{V_C^N} G_{0T}\left(\mathbf{x}\right)\right\|_2^2 + \left\|P_{V_R^N} G_{0R}\left(\mathbf{x}\right)\right\|_2^2\right]^{-1} \\ &= \left[\sum_{k=M+1}^{\min(N_t,N_r)} \left(\left|\mu_k^T G_{0T}\left(\mathbf{x}\right)\right|^2 + \left|\nu_k^\dagger G_{0R}\left(\mathbf{x}\right)\right|^2\right)\right]^{-1} \end{aligned} \tag{12}$$

In Eq. (12), the two parts besides the sum sign are also called transmitting mode and receiving mode respectively. Thus, Eq. (10) for transducer array can be replaced by

$$\begin{aligned} I\left(\mathbf{x}\right) &= \left[\left\|P_{V_C^N} G_0\left(\mathbf{x}\right)\right\|_2^2 + \left\|P_{V_R^N} G_0\left(\mathbf{x}\right)\right\|_2^2\right]^{-1} \\ &= \left[\sum_{k=M+1}^{N} \left(\left|\mu_k^T G_0\left(\mathbf{x}\right)\right|^2 + \left|\nu_k^\dagger G_0\left(\mathbf{x}\right)\right|^2\right)\right]^{-1} \end{aligned} \tag{13}$$

because the receiver and transmitter arrays are the same and so are their illumination vectors.

2.3. TR-MUSIC Algorithm for Extended Targets

As mentioned above, for point targets with $M < N$, $\mathbf{H} \in \mathbb{C}^{N\times N}$ is rank deficient and the number of singular values and singular vectors of $\mathbf{H}$ will equal to the number of targets M in a one-by-one manner. TR-MUSIC imaging function will work very well. But when the object is penetrable or its size compares to the wavelength, it cannot be seen as a point target but an extended target. This is true in practical circumstances such as breast cancer detection and diagnostic application.

For extended targets, generally $\mathbf{H}$ is a matrix with full rank. This means $Q = N$, and the imaging function $I(\mathbf{x})$ cannot be calculated directly from Eq. (10) or Eq. (13). At this time, the singular value spectrum curve no longer drops sharply at certain point but decreases much slowly. Each singular value indicates an independent contribution to the total scattered energy from a scattering centre or bright spot. Furthermore, as Hou et al. presented in [13], the peaks of the imaging function maybe exist on the target boundary or inside of the object due to physical resonance. There is no distinct boundary between signal subspace and noise subspace. But the TR-MUSIC method can be still applied to extended target imaging with degraded performance [13, 14] and can be used to sketch the shape of extended targets, which will be demonstrated in the simulation examples later.

To apply TR-MUSIC for extended targets, the key issue is how to decide the best boundary between signal subspace and noise subspace, i.e., optimal value of M, to obtain the best imaging result if the array element number is big enough. To resolve this problem, Marengo et al. took the "knee" of the singular values spectrum in logarithmic scale as the boundary point to pick the principal components out from the noised signal subspace [14]. And Hou et al. proposed a more complicated thresholding strategy for regularization based on resolution and noise level, but multiple-frequency data is needed.

According to our numerical tests using the scattered data of simple extended targets from FDTD simulations, the acceptable imaging results happen at multiple boundary points rather than only at one specific point, and that at the most times these boundary points are not the "knee" of the singular value spectrum. The super-resolution property of TR-MUSIC can guarantee a good imaging even only from single-frequency data. Therefore, we propose a new double-thresholding strategy based on energy estimation to decide the best boundary region between effective signal subspace and noise subspace, and combine all the effective boundary points together to obtain a clearer imaging of illuminated region.

The total energy involved in $\mathbf{H}$ can be estimated by the square of

its Frobenius norm, defined by

$$\|\mathbf{H}\|_F^2 = \sum_{i=1}^{N}\sum_{j=1}^{N}|h_{ij}|^2 = \text{trace}\left(\mathbf{H}\mathbf{H}^\dagger\right) = \sum_{i=1}^{N}\sigma_i^2 \tag{14}$$

As Hou et al. did in Ref. [13], define the signal subspace part of $\mathbf{H} = \mathbf{U}\mathbf{\Sigma}\mathbf{V}^\dagger$ by

$$\mathbf{H}_{\text{signal}} = \mathbf{U}_M\mathbf{\Sigma}_M\mathbf{V}_M^\dagger \tag{15}$$

where M is the supposed estimation of the boundary between signal subspace and noise subspace, $\mathbf{U}_M$ and $\mathbf{V}_M$ denoting the first M columns of $\mathbf{U}$ and $\mathbf{V}$, respectively. The energy ratio (ER) of the signal subspace to the total energy of $\mathbf{H}$ is

$$\text{ER} = \frac{\|\mathbf{H}_{\text{signal}}\|_F^2}{\|\mathbf{H}\|_F^2} = \frac{\sum_{i=1}^{M}\sigma_i^2}{\sum_{i=1}^{N}\sigma_i^2} \tag{16}$$

The parameter ER can be used to judge the performance of the estimated M value. The fact that ER is too low shows that M value is too small to extract all the dominating contribution of main bright spots on the target from $\mathbf{H}$. On the other hand, The fact that ER is too high shows that M value is too big to reject the numerical or background noise in $\mathbf{H}$. Double-thresholding strategy for ER is an acceptable choice

$$\text{ER}_{\min} \le \text{ER} \le \text{ER}_{\max} \tag{17}$$

where $\text{ER}_{\min}$ denotes the lower thresholding and $\text{ER}_{\max}$ the higher thresholding. All the M values satisfying Eq. (17) consist a acceptable zone called B. Combining all the acceptable M values, the imaging function becomes

$$I(\mathbf{x}) = \sum_{b\in B}\left[\sum_{k=b+1}^{N}\left(\left|\nu_k^\dagger G_0(\mathbf{x})\right|^2 + \left|\mu_k^T G_0(\mathbf{x})\right|^2\right)\right]^{-1} \tag{18}$$

This is called the double-thresholding strategy based on energy estimation for TR-MUSIC imaging algorithm. The values of two thresholding can be decided by the noise performance of the imaging system. This imaging function can give clearer image than that in Eq. (13) which only utilizes one M value. If the raw data includes multiple frequencies or broad band, the extra information can be combined together by

$$I(\mathbf{x}) = \sum_{f}\sum_{b\in B}\left[\sum_{k=b+1}^{N}\left(\left|\nu_k^\dagger G_0(\mathbf{x})\right|^2 + \left|\mu_k^T G_0(\mathbf{x})\right|^2\right)\right]^{-1} \tag{19}$$

3. SIMULATIONS AND DISCUSSIONS

All the following simulations resolve the electromagnetic scattering of 2D objects with air as the background media for clearness and simplicity although the TR-MUSIC algorithm can be applied to 3D targets. The scattering data is obtained from 2D FDTD codes except the multiple point targets which are calculated directly from Green's function. In the 2D FDTD simulation, space step size is $\Delta x = \Delta y = 0.5\,\text{cm}$, simulated space is 200×200, time step size is $\Delta t = 5 \times 10^{-12}\,\text{s}$, and simulated time steps are 1024. The exciting signal is Gaussian modulated continuous wave, whose center frequency is 3 GHz and pulse half width is $10\Delta t$. To avoid the receiving antenna's effect on the imaging algorithm, the scattered fields on observation points are directly taken as the received waveforms. The frequency domain data is obtained by the DFT of the scattered time domain waveforms.

3.1. Multiple Point Targets

In this example, the five point targets locate at $(-10, 0)$, $(-1, 0)$, $(1, 0)$, $(-10, -10)$ and $(0, -10)$, respectively, as shown in Fig. 2. The imaging region is $30\,\text{cm} \times 30\,\text{cm}$ and the number of array elements $N = 14$. The distance from the centre of imaging region to the circle antenna array element is $R = 30\,\text{cm}$. $\mathbf{H}$ is calculated directly by 2D Green's function $H_0^{(2)}(\beta\rho)$, i.e., the zero order Hankel function of the second kind, where $\beta = 2\pi/\lambda$ is the wave number of free space, ρ denotes the distance between field point and source point. The frequency is 3 GHz, wavelength $\lambda = 10\,\text{cm}$ and $M = 5$. The normalized singular value distribution spectrum and the imaging function $I(\mathbf{x})$ in 2D and 3D views are displayed in Figure 2, respectively. Obviously the number of point targets equals to the number of non-zero singular values if the numerical error lower than $-350\,\text{dB}$ is neglected. It can also be observed that the TR-MUSIC algorithm can resolve the five point targets completely even when the smallest distance, 2 cm, is less than $\lambda/4$. This super-resolution is obtained only from the single frequency scattering data, and better resolution can be expected from multiple frequencies or wide-band data.

3.2. Rectangle Metal Cylinder

The first extended target is a rectangle metal cylinder whose dimension is $20\,\text{cm} \times 10\,\text{cm}$, i.e., $2\lambda \times \lambda$ for 3 GHz frequency. The imaging region is $30\,\text{cm} \times 30\,\text{cm}$ and the number of array elements $N = 14$. The size of the circle antenna array keeps the same, $R = 30\,\text{cm}$. The normalized singular value spectrum and imaging results for different M values are

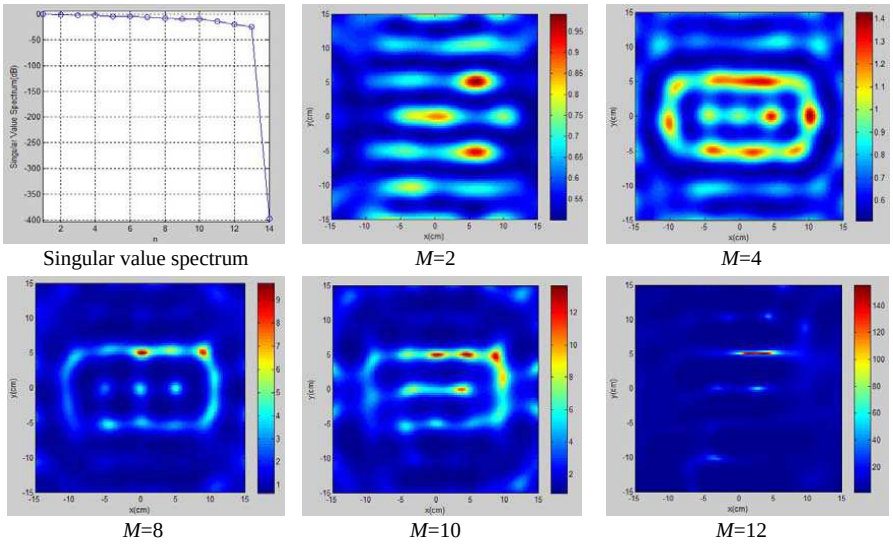

Figure 3. Singular value spectrum and imaging results of rectangle metal cylinder ($N = 14$, $f = 3\,\text{GHz}$).

shown in Figure 3. Comparing with that of point targets in Figure 2(a), the singular value spectrum for extended targets decreases slower and imaging bright spots don't correspond to the "bigger" singular values one-to-one again. The imaging results for $M = 2$, 4, 8, 10 and 12 are given from top middle to bottom right, respectively. It can be seen that the imaging results vary with M values and the image peaks or bright spots locate on the boundary of or inside the metal. Therefore, the correct choice for M value, the boundary between signal subspace and noise subspace, is very important to a good TR-MUSIC image of an extended target and it can sketch the shape of the illuminated objects because "large" targets can be represented by their main scattering centres as radar target characteristics.

When the number of array elements changes to 40, i.e., $N = 40$, the normalized singular value spectra and imaging results of the same rectangle metal cylinder with frequency = 2, 3 and 4 GHz are shown in Figure 4, Figure 5 and Figure 6, respectively. When the number of antennas is greater than that of distinguishable bright spots on the target, the slow decreasing characteristics of singular value spectrum for extended targets becomes clearer. Furthermore, the higher the detecting frequency, the more the distinguishable bright spots. This means that the smaller the wavelength, the higher the resolution of TR-MUSIC algorithm. From these imaging results it can be concluded

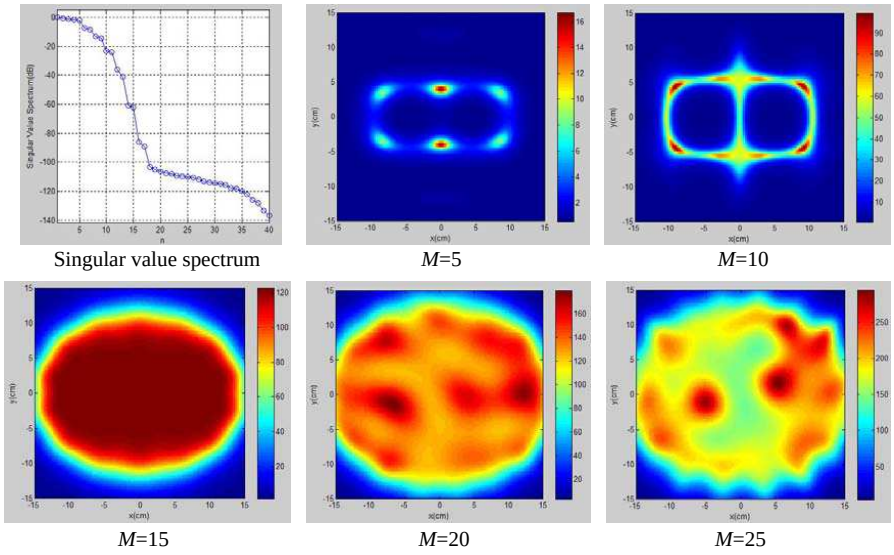

Figure 4. Singular value spectrum and imaging results of rectangle metal cylinder ($N = 40$, $f = 2\,\text{GHz}$).

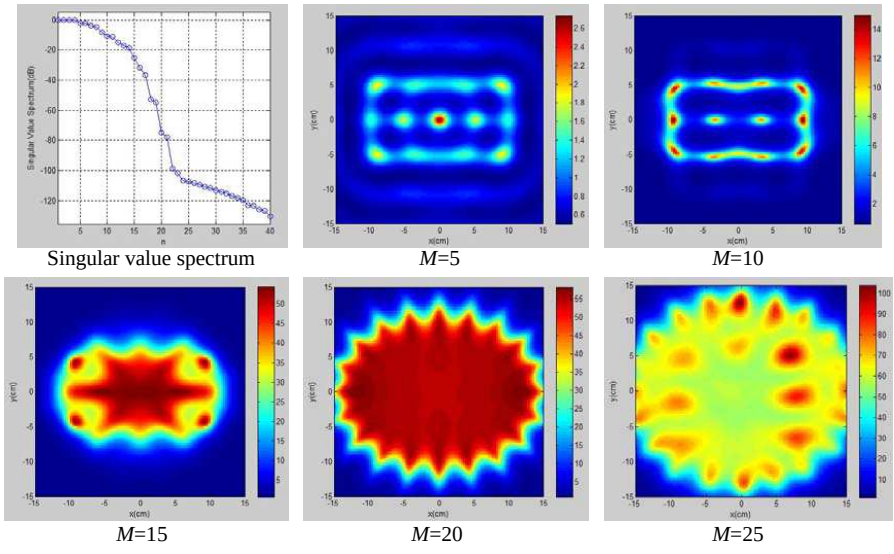

Figure 5. Singular value spectrum and imaging results of rectangle metal cylinder ($N = 40$, $f = 3\,\text{GHz}$).

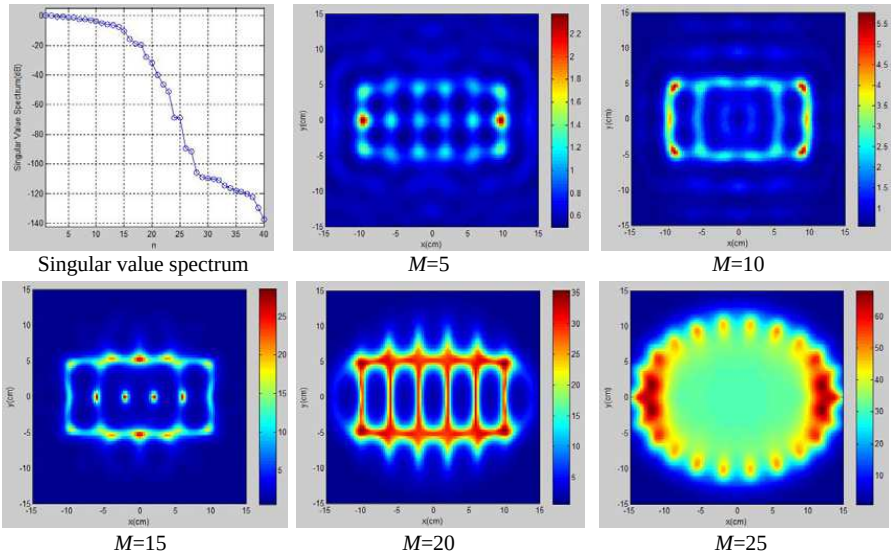

Figure 6. Singular value spectrum and imaging results of rectangle metal cylinder ($N = 40$, $f = 4\,\mathrm{GHz}$).

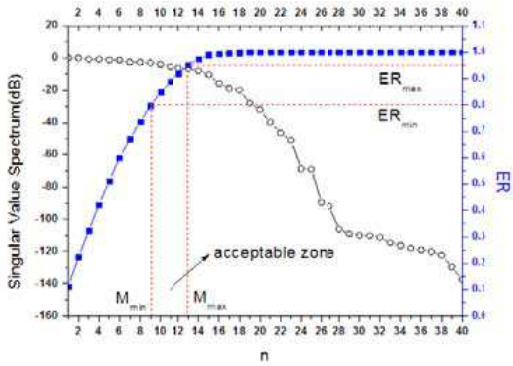

Figure 7. Double-thresholding strategy.

that the choice of M value is very important for a good imaging.

To illustrate our double-thresholding strategy for the choice of optimal M values, taking the data with $N = 40$ and $f = 4\,\mathrm{GHz}$ as an example, its normalized singular value spectrum and corresponding ER curve are given in the left part of Figure 7. By choosing $\mathrm{ER}_{\min} = 0.8$ and $\mathrm{ER}_{\max} = 0.95$, they correspond $M_{\min}$ and $M_{\max}$ on the ER

curve, respectively. The interval between $M_{\min}$ and $M_{\max}$ is called acceptable zone. All the M values in this zone are used as the optimal boundary of signal subspace and noise subspace respectively and all the obtained images are combined to get the optimal imaging as does in Eq. (18). For the data of 2 GHz, the optimal M values are 5 and 6. For 3 GHz data, the M values are 7, 8 and 9. And for 4 GHz data, the M values are 10, 11 and 12. It can be seen that the ratio of the first optimal M value to the frequency almost keep invariant as S. Hou et al. have figured out in [13]. The optimal imaging results are given in Figure 8 for these single frequencies and multi-frequency, respectively. In Figure 8, the last imaging from multi-frequency data of 2 GHz, 3 GHz and 4 GHz is constructed using Eq. (19), which shows that the multi-frequency or broadband data fusion can get more shape details about the illuminated targets because of more information and increased resolution.

In practical applications, there is always error or noise in the raw simulated or sampled data. To test the imaging capability against noise of this energy estimation based TR-MUSIC algorithm, artificial amplitude and phase noise are gradually added on to the raw simulated

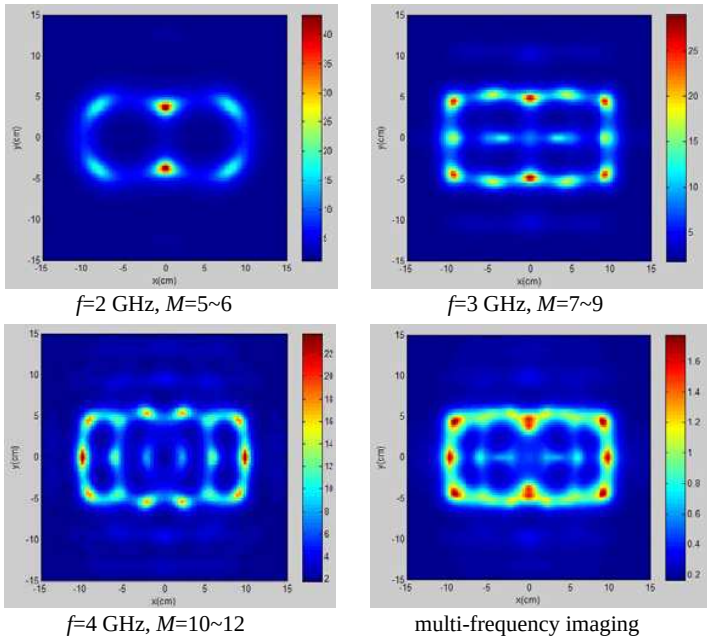

Figure 8. Optimal imaging results for rectangle metal cylinder based on double-thresholding strategy.

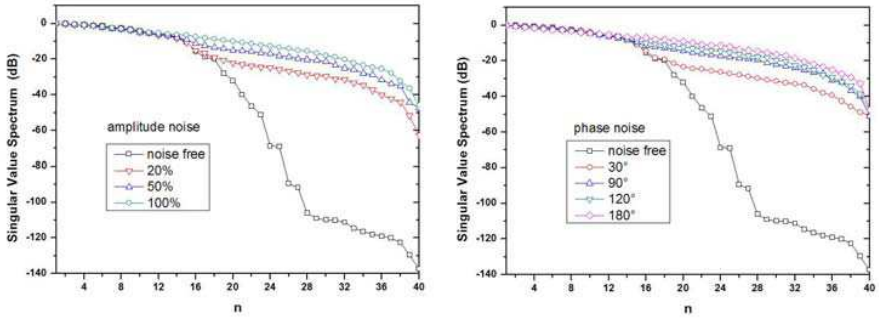

Figure 9. Noise impact on singular value spectrum ($f = 4\,\text{GHz}$).

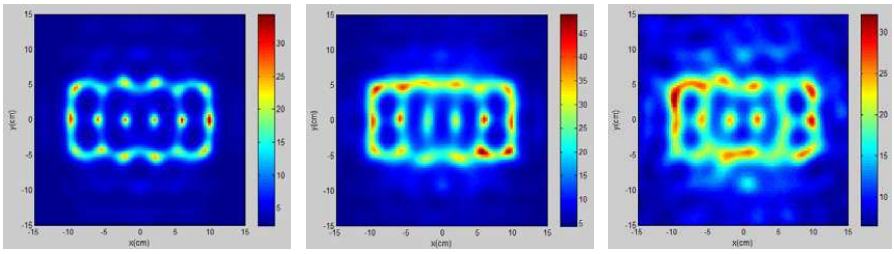

20%, M=10~13 50%, M=11~17 100%, M=14~22

Figure 10. Amplitude noise impact on the imaging results.

data of $f = 4\,\text{GHz}$ and $N = 40$. The added amplitude noise is random Gaussian noise with a zero mean and deviations of 20%, 50% and 100%, respectively. And the added phase noise is random uniform distribution noise with interval 30°, 90°, 120° and 180°, respectively. The impact of noise on the normalized singular value spectrum is shown in Figure 9. It can be seen that the noise mainly increases the last part of the singular value spectrum and makes the curve smoother. That is, the noise plays more impact on the noise subspace but not on the signal subspace. Keeping the double-thresholding the same as before, i.e., $\text{ER}_{\min} = 0.8$ and $\text{ER}_{\max} = 0.95$, the imaging results under these amplitude noise and phase noise are listed in Figure 10 and Figure 11, respectively. Comparing to the noise-free imaging of $f = 4\,\text{GHz}$ in Figure 8, these imaging results deteriorate gradually as the noise increases and the optimal M values increase accordingly. But the TR-MUSIC algorithm based on energy estimation can give recognizable imaging results even with 100% amplitude noise or 180° phase deviation. This proves its super-resolution imaging and outstanding noise rejection capability.

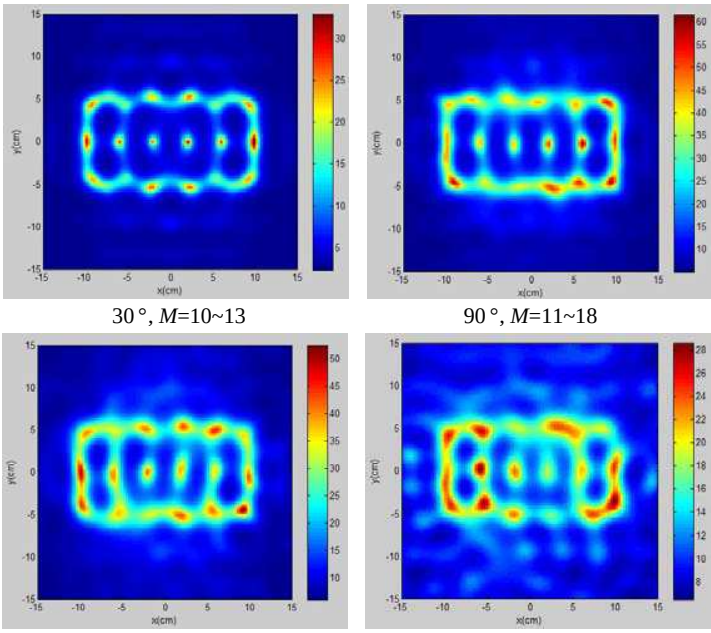

Figure 11. Phase noise impact on the imaging results.

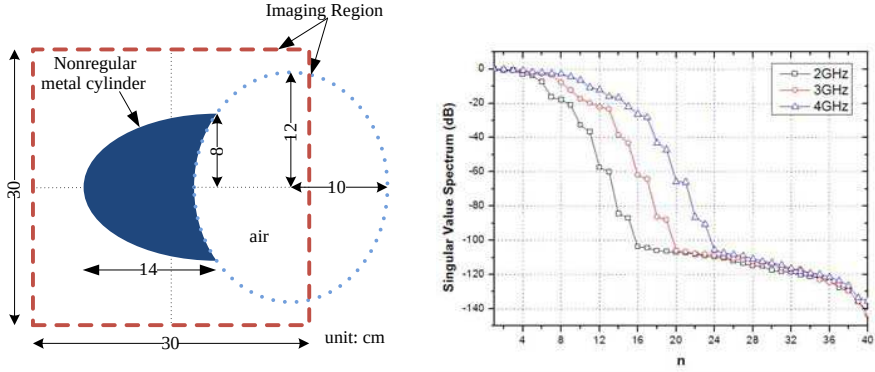

Figure 12. Irregular metal cylinder and its singular value spectrum.

3.3. Irregular Metal Cylinder

The second extended target is an irregular metal cylinder whose shape detail is sketched in the left part of Figure 12. All the other parameters are the same as the rectangle metal cylinder discussed in the previous example, i.e., $N = 40$, $R = 30\,\text{cm}$, $\text{ER}_{\min} = 0.8$ and $\text{ER}_{\max} = 0.95$. Its

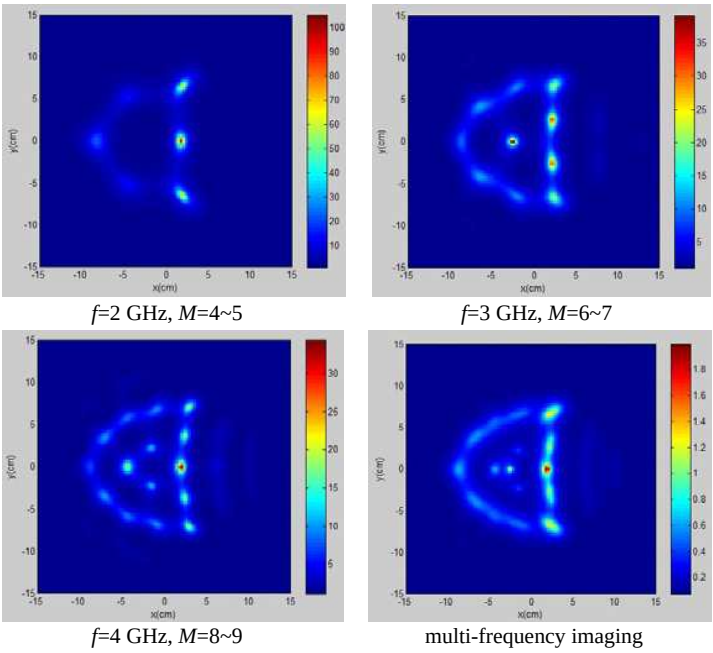

Figure 13. Optimal imaging results for irregular metal cylinder based on double-thresholding strategy.

singular value spectrum is shown in the right part of Figure 12 and the optimal imaging results at each single frequency and mutli-frequency are given in Figure 13. The phenomena and conclusions mentioned above are demonstrated once more and no further explanation is needed.

4. CONCLUSIONS

From the above simulations and demonstrations above, it can be concluded that the proposed double-thresholding strategy based on energy estimation is a simple and effective method in terms of choosing the accurate boundary between the signal subspace and noise subspace in the TR-MUSIC algorithm for microwave imaging of extended targets. The new TR-MUSIC algorithm based on energy estimation can give recognizable imaging results even with 100% Gaussian amplitude noise or uniform distribution 180° phase deviation.This algorithm accompanies with strong noise rejection and super-resolution capability and can be used to microwave imaging for extended targets

in many practical applications such as medical diagnostics and port security check. Further work is needed to focus on 3D and dielectric targets imaging using this algorithm and experimental system building-up.

REFERENCES

1. Siegel, R., E. Ward, O. Brawley, and A. Jemal, "Cancer statistics, 2011: The impact of eliminating socioeconomic and racial disparities on premature caner dealths," *CA Caner. J. Clin.*, Vol. 61, No. 4, 212–236, 2011.
2. Hassan, A. M. and M. El-Shenawee, "Review of electromagnetic techniques for breast cancer detection," *IEEE Reviews in Biomedical Engineering*, Vol. 4, 103–118, 2010.
3. Fear, E. C., P. M. Meaney, and M. A. Stuchly, "Microwaves for breast cancer detection," *IEEE Potentials*, Vol. 22, No. 1, 12–18, 2003.
4. Flores-Tapia, D., G. Thomas, and S. Pistorius, "An improved wavefront reconstruction method for breast microwave imaging," *31st Annual International Conference of the IEEE EMBS Minneapolis*, Minnesota, USA, Sep. 2–6, 2009.
5. Klemm, M., I. J. Craddock, J. A. Leendertz, A. Preece, and R. Benjamin, "Radar-based breast cancer detection using a hemispherical antenna array — Experimental results," *IEEE Trans. Antennas Propag.*, Vol. 57, No. 6, 1692–1704, Jun. 2009.
6. Li, X. and S. C. Hagness, "A confocal microwave imaging algorithm for breast cancer detection," *IEEE Microwave and Wireless Components Letters*, Vol. 11, No. 3, 130–132, 2001.
7. Fear, E. C., X. Li, S. C. Hagness, and M. A. Stuchly, "Confocal microwave imaging for breast cancer detection: Localization of tumors in three dimensions," *IEEE Transactions on Biomedical Engineering*, Vol. 49, No. 8, 812–822, 2002.
8. O'Halloran, M., E. Jones, and M. Glavin, "Quasi-multistatic MIST beamforming for the early detection of breast cancer," *IEEE Transactions on Biomedical Engineering*, Vol. 57, No. 4, 830–840, Apr. 2010.
9. Chen, Y., I. J. Craddock, and P. Kosmas, "Multiple-input multiple-output radar for lesion classification in ultrawideband breast imaging," *IEEE J. Selected Topics in Signal Processing*, Vol. 4, No. 1, 187–201, Feb. 2010.
10. Lev-Ari, H. and A. J. Devaney, "The time-reversal technique re-interpreted: Subspace-based signal processing for multi-static

target location," *Proceedings of the 2000 IEEE Sensor Array and Multichannel Signal Processing Workshop*, 509–513, 2000.

11. Gruber, F. K., E. A. Margengo, and A. J. Devaney, "Time-reversal imaging with multiple signal classification considering multiple scattering between the targets," *J. Acoust. Soc. Amer.*, Vol. 115, 3042–3047, 2004.
12. Devaney, A. J., E. A. Margengo, and F. K. Gruber, "Time-reversal-based imaging and inverse scattering of multiply scattering point targets," *J. Acoust. Soc. Amer.*, Vol. 118, 3129–3138, 2005.
13. Hou, S., K. Solna, and H. Zhao, "A direct imaging algorithm for extended targets," *Inv. Probl.*, Vol. 22, 1151–1178, 2006.
14. Marengo, E. A., F. K. Gruber, and F. Simonetti, "Time-reversal MUSIC imaging of extended targets," *IEEE Trans. Image Processing*, Vol. 16, No. 8, 1967–1984, Aug. 2007.
15. Zhang, W. and A. Hoorfar, "Through-the-wall target location with time reversal MUSIC method," *Progress In Electromagnetics Research*, Vol. 106, 75–89, 2010.
16. Liu, X.-F., B.-Z. Wang, and J. L.-W. Li, "Transmitting-mode time reversal imaging using MUSIC algorithm for surveillance in wireless sensor network," *IEEE Trans. Antennas Propag.*, Vol. 60, No. 1, 220–230, Jan. 2012.
17. Lehmana, S. K. and A. J. Devaney, "Transmission mode time-reversal super-resolution imaging," *J. Acoust. Soc. Am.*, Vol. 113, No. 5, 2742–2753, May 2003.
18. Strang, G., *Introduction to Linear Algebra,* 3rd Edition, Wellesley-Cambridge Press, 2003.
19. Trefethen, L. N. and D. Bau, *Numerical Linear Algebra,* The Society of Industrial and Applied Mathematics, 1997.
20. Marengo, E. A. and F. K. Gruber, "Subspace-based localization and inverse scattering of multiply scattering point targets," *EURASIP Journal on Advances in Signal Processing,* Vol. 2007, Article ID 17342, 2007, doi:10.1155/2007/17342.